Composite Structures 272 (2021) 114197

Contents lists available at ScienceDirect

Composite Structures

journal homepage: www.elsevier.com/locate/compstruct

Effect of saw-tooth ply drops on the mechanical performance of tapered composite laminates

Wilhelm Woigk [a,b,*,1], Bing Zhang [a], Mike I. Jones [a], Moritz Kuhtz [b], Andreas Hornig [b], Maik Gude [b], Stephen R. Hallett [a,*]

[a] Bristol Composites Institute, University of Bristol, University Walk, Bristol BS8 1TR, UK
[b] Technische Universität Dresden, Institute of Lightweight Engineering and Polymer Technology (ILK), Holbeinstr. 3, 01307 Dresden, Germany

ARTICLE INFO

Keywords:
Automated fibre placement
Ply drops
Stress concentrations
Delamination

ABSTRACT

Automated Fibre Placement (AFP) is a manufacturing technique to produce large, high quality composite parts, where preimpregnated carbon fibre tapes are laid side-by-side to generate the composite preform. Thickness changes within a component are realised through internal ply terminations, with the tapes being cut perpendicular to the fibre direction. In plies laid up at an angle to the taper direction, the AFP tape cuts create saw-tooth shaped ply drop tips. This increases the size of resin rich zones and enlarges the region where stress concentrations and cracks can develop, which amplifies the risk of failure. This study investigates the effect of simulated AFP saw-tooth ply drop tips, created by hand layup, on the mechanical properties and failure behaviour of carbon fibre/epoxy composites and compares its results to reference broad goods layups. The stiffness was found to be unaffected and the strength was reduced by ~ 10%. The failure mode was governed by delamination for the saw-tooth ply drop tips, whereas the reference specimens failed by rupture of the unidirectional fibres. A finite element modelling technique was used to select the layup to be tested. The models were then refined in the light of experimental results, to accurately predict the failure and explain the failure mode transition.

1. Introduction

High performance composite materials have been gaining interest in many industrial fields such as aviation, automotive and the renewable energy sector. Today, passenger aircrafts contain up to 50% of carbon fibre-reinforced plastics including primary structures such as fuselage and wings. Such large components can only be manufactured using automated processes. Two main technologies have proven to be very effective to produce large laminated composites for applications in primary structures; Automated Fibre Placement (AFP) and Automated Tape Lay-Up (ATL). These technologies are employed today to manufacture structural composite laminates from preimpregnated fibres or unidirectional (UD) tapes [1–6].

In order to meet design requirements and to allow for more significant weight savings, tapered composites are widely used, e.g. in the root of helicopter rotors or aircraft engine fan blades. Tapered composites are characterised by thickness changes within the structure formed by ply terminations, also known as ply drops [7–9]. In AFP manufactured composites, a variation in thickness is usually performed in discrete steps by cutting the narrow tapes and allowing the tips to be inside the part, creating structural inhomogeneities [10]. The load carried by the terminating plies is transferred to the continuous plies by the matrix material surrounding the ply drop tips. This load transfer gives rise to interlaminar shear and out-of-plane direct stresses, making the composite locally susceptible to early damage [11–15]. Delamination, crack growth and fibre failure can occur at comparatively low global stresses, which can be considerably lower than the constituents' strengths [16,17]. Many studies have been carried out in the past on the failure behaviour of tapered composites in order to develop design guidelines with the goal to increase the damage resistance [9,18–20]. Those guidelines have usually been deduced from strength and fracture mechanics experiments [7,12,16,21], in which delamination was the dominant failure mechanism.

Along with the development of interlaminar stresses, resin rich zones are created in front of the dropped plies, which act, due to the significantly lower mechanical properties compared to the prepreg

* Corresponding authors.
E-mail addresses: wilhelm.woigk@mat.ethz.ch (W. Woigk), stephen.hallett@bristol.ac.uk (S.R. Hallett).
[1] Current Address: Complex Materials, Department of Materials, ETH Zürich, Vladimir-Prelog-Weg 5, 8093 Zurich, Switzerland.

https://doi.org/10.1016/j.compstruct.2021.114197
Received 16 March 2021; Revised 26 May 2021; Accepted 27 May 2021
Available online 29 May 2021

fibre plies, as crack initiators [7,9,15,22]. However, to what extent the resin pocket and their geometry contribute to the damage initiation is seldom discussed in the literature. Particularly accumulations of resin rich zones associated with the fibre path deviations in the vicinity of such resin rich zones can have an effect on the failure behaviour of carbon fibre-reinforced epoxy composites [6]. Vizzini [11] studied interlaminar stress distributions on ply drop formations and found that asymmetric and in particular non-triangular shaped resin pockets increase the stress state. Vidyashankar and Murty [17] also concluded in their study that the size of the resin pocket is a crucial parameter that influences the nature of the stress distribution around the tip of a ply drop. However, these two papers consider geometrical variations of the resin pocket in the longitudinal plane, whereas the influence of geometrical changes in the width direction remain unclear.

More recently, Zhang et al. [15] developed high-fidelity models capable of accurately predicting both the failure mode and strength of modestly and severely tapered composites subjected to tensile loading. The authors systematically studied the effect of cohesive strength pairs considering a mixed-mode failure criterion with contributions of mode I (opening) and mode II (shearing) failure. It was found that enhanced cohesive properties due to through-thickness compression during loading and cohesive strength pair values being closer to realistic properties led to a better description of the laminate behaviour.

This study aims to investigate the effect of realistic AFP off-axis ply drop formations, referred to as saw-tooth ply drop tips, on the mechanical performance and the failure behaviour of carbon fibre-reinforced epoxy composites with a geometrical taper. The analysis techniques developed by Zhang et al. [15] were used to study various stacking sequences and ply drop configurations to determine a particular layup that exhibits delamination failure initiation at a ± 45° ply drop with a saw-tooth pattern. After experimental tests, updates were made to the numerical models to show that improvement could be achieved in the level of correlation. The numerical study along with the experimental validation gives insight into how realistic ply drop formations affect the tensile properties of simulated AFP composite laminates and if manufacturing processes need adjustments to obtain the best performance for tapered composites in structural applications.

2. Materials and methods

2.1. Composite layup development

The layups studied in this research were designed using numerical tools developed by Zhang et al. [15] in the non-linear explicit finite element (FE) solver LS-Dyna. These tools allow for a high-fidelity analysis to model delamination in tapered laminates with internal ply drops. Bespoke meshing algorithms were used to create a variety of layups in order to study the effect of realistic ply drop tips. The layup can be designed in a way that delamination failure precedes fibre failure where simulated interlaminar stresses are highest at + 45° or −45° ply drop tips. These ply-drop tips will exhibit a saw-tooth pattern, whereas the 0° and 90° ply drop tips will have straight tips. In the simulations, all ply drop tips were constructed with straight edges, i.e. no saw-tooth pattern, as the modelling tools [15] were originally developed for broad goods composites. However, the results are still useful here for layup selection. In order to initiate the delamination failure at ± 45° ply drops, the interlaminar stresses at the 0° ply tips were required to be considerably lower than at the ± 45° tips. Furthermore, 90° plies were not considered in the layup because of their propensity to develop transverse matrix cracks at relatively low global stresses, which may significantly influence the failure mode of the specimens. To allow for a gradual transition from the thick to the thin section, a 16-ply laminate was reduced to 8 plies by terminating 8 of the thick section plies, separated by a nominal stagger distance of 2 mm.

2.2. Finite element modelling and failure analysis

High-fidelity finite element (FE) models were used to evaluate eight developed stacking sequences (see Fig. 4, further explanation follows in Section 3.1). The FE mesh was created by custom written algorithms developed in Matlab® [13,15], with one single-integration solid element through the thickness of each ply, i.e. thickness of 0.25 mm. Along the specimen length, the elements were 0.1 mm long in the critical region and gradually increased to 3 mm away from the taper. In the transverse direction, the elements had a constant size of 0.5 mm, whereas the full laminate width of 35 mm was described. To obtain a delamination failure, special attention was paid to the model's failure mode and the location of damage initiation.

The interface behaviour was modelled using cohesive zone model (CZM) interface elements with 0.01 mm thickness, which followed a mixed-mode bilinear softening law. For damage initiation, the strength based quadratic criterion was [3,23]:

$$\left(\frac{\langle \sigma_I \rangle}{S_I}\right)^2 + \left(\frac{\sigma_{II}}{S_{II,E}}\right)^2 = 1 \tag{1}$$

where σ_I and σ_{II} are mode I and mode II stresses, S_I and $S_{II,E}$ are mode I and enhanced mode II strengths. $\langle\rangle$ is the Macaulay operator, which takes only positive values and ignores negative (compressive) stresses. Due to the occurrence of through-thickness compression stresses during tensile loading of composites with a geometrical taper, the mode II shear strength, S_{II}, increases. This enhancement is taken into account by a dimensionless through-thickness enhancement factor, η_f, which is multiplied by the acting through-thickness stress [24]:

$$S_{II,E} = S_{II} - \eta_f \cdot \min(0, \sigma_I) \tag{2}$$

After the criterion in Equation (1) is met, failure is initiated, and the interface strength is degraded linearly until complete interface failure. To model this damage progression, a fracture energy based criterion for mixed-mode interactions was used [3,23]:

$$\left(\frac{G_I}{G_{IC}}\right) + \left(\frac{G_{II}}{G_{IIC,E}}\right) = 1 \tag{3}$$

where G_I and G_{II} are mode I and mode II fracture energies, G_{IC} is the mode I critical energy release rate and $G_{IIC,E}$ is the enhanced mode II critical energy release rate due to the through-thickness compression [15] and is determined by:

$$G_{IIC,E} = \left(\frac{S_{II,E}}{S_{II}}\right)^2 \cdot G_{IIC} \tag{4}$$

The simulation contained two loading steps: a thermal step to account for residual stresses from the manufacturing and a tensile loading step that represents the mechanical test. The thermal step was realised through a temperature difference of −160 °C, applied over the first 0.5 s of the analysis time. The tensile step was then carried out via a displacement-controlled velocity of 2.2 mm/s. Elastic, thermal and interface material properties for solid and cohesive zone elements are summarised in Tables 1 and 2, respectively.

Table 1
Elastic and thermal properties for unidirectional IM7/8552 laminates [15,25].

E_{11} (MPa)	E_{22} (MPa)	E_{33} (MPa)	ν_{12} (−)	ν_{13} (−)	ν_{23} (−)	G_{12} (MPa)	G_{13} (MPa)	G_{23} (MPa)	α_{11} (mm/K)	α_{22} (mm/K)	α_{33} (mm/K)
161,000	11,380	11,380	0.32	0.32	0.45	5170	5170	3920	0.0	1×10^{-5}	1×10^{-5}

Table 2
Interface properties for unidirectional IM7/8552 laminates [15,25].

G_{IC} (N/mm)	G_{IIC} (N/mm)	S_I (MPa)	S_{II} (MPa)	E_I (N/mm^3)	E_{II} (N/mm^3)
0.2	0.8	90	110	4.67 × 10^5	1.75 × 10^5

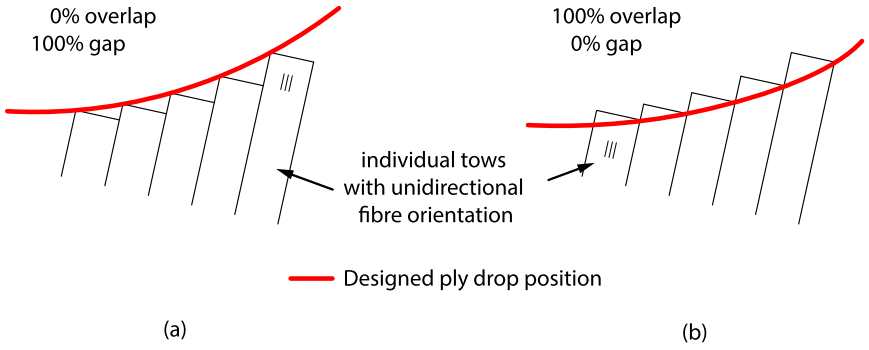

Fig. 1. Cut ply distribution along a tow drop off path (indicated by the red line). Shown are the two extreme cases. Any overlap/gap ratio between these two extrema is imaginable (). adapted from [1]

2.3. Materials and specimen manufacture

Unidirectional (UD) carbon fibre preimpregnated material, HexPly IM7/8552 by Hexcel™, was used to manufacture the composite laminates. Cutting layouts were developed as described previously [6]. The position and the pattern of ply drop tips with a saw-tooth pattern can be engineered in various ways. The nominal position of the tip can be completely free or fully covered by the dropped ply, leading to 100% gap (Fig. 1(a)) or 100% overlap (Fig. 1(b)) scenario. Theoretically, any coverage between these two extrema can be realised. In this study, the method of 100% gap was selected to create the saw-tooth pattern of the ply drops.

The laminates were manufactured via a manual layup of preimpregnated plies. To create realistic layers built out of parallel tows, as they would be fabricated in an automated process, the material was cut into individual tows. However, to still allow for a fast lab-scale manufacturing of the laminates, the individual tows were still attached on one side of the layers (see Fig. 2(a)). Therefore, the layers were divided into the “strip free length” and the “strip length”. As shown schematically, the strip free length was maintained to be within the length covered by the end tabs of the tensile specimen, thus having no influence on the mechanical performance. The strip length was then determined in accordance with the design of the dropped ply. To guarantee the coverage of the full width of the composite panel with the strips, the width of the ply had to be increased, which was done by extending the ply width by the “added length”. With the manual approach, a precise positioning of the ply drop features could be assured.

Fig. 2(b) shows the ply drop pattern during the hand layup. The saw-tooth pattern of dropped plies which lies underneath a continuous 0° layer can be seen by the alternation of matt and shiny surfaces, whereas the trajectory of the ply drop tip is indicated by the red zig-zag line. During the layup, the laminates were consolidated under vacuum after each ply to eliminate entrapped air between the layers. Composite curing was done in an autoclave, LBBC (United Kingdom), using Hexcel’s recommended curing cycle [26]. To avoid possible differences in the curing process, all laminates were cured in the same cycle. The tapered specimens with a symmetric geometry were cured as two separate halves and subsequently bonded back-to-back using a 3M™ AF163-2 structural adhesive film. The bonding was carried out under vacuum for 100 min at 120 °C. Two-sided tapered panels were equipped with glass fibre-reinforced epoxy end tabs bonded onto

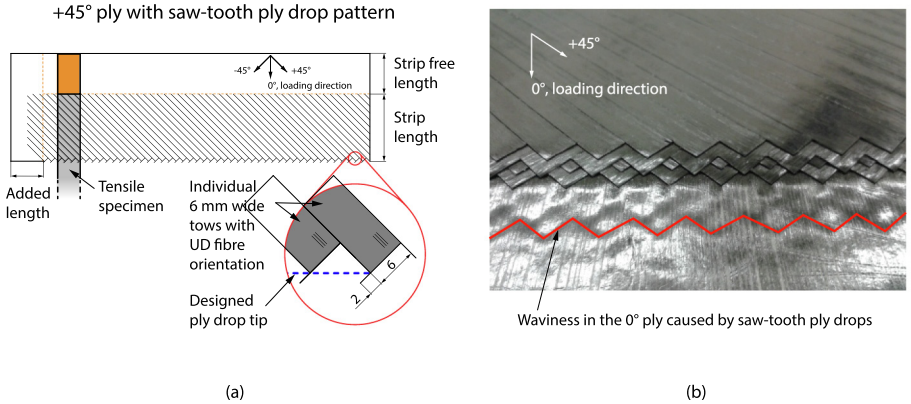

Fig. 2. (a) Cutting layout of a saw-tooth + 45° ply to simulate individual unidirectional (UD) strips). (b) Saw-tooth ply drop pattern during the layup.

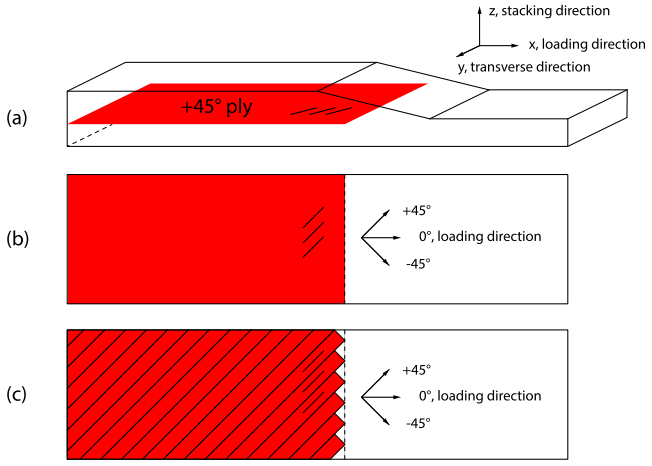

Fig. 3. Schematic of ply drops along a defined path perpendicular to the loading direction. (a) 3D illustration of the ply drop, (b) top view of a straight ply drop and (c) top view of a saw-tooth ply drop.

both sides at each end of the plate. Tensile specimens with a size of 250 mm × 35 mm were extracted from this plate using a cutting machine with a diamond-coated saw blade.

Two different types of composites were produced: a straight and a saw-tooth configuration. Fig. 3 illustrates schematically the two designs for a + 45° ply.

2.4. Mechanical testing

Tensile tests were carried out in accordance with ASTM D3039 [27]. The nominal thicknesses of the specimens were 4 mm and 8 mm for the thin and thick sections of the taper, respectively. The specimens had a gauge length of 150 mm. Tests were carried out at ambient temperature using a servo-hydraulic Instron universal material testing machine equipped with a 250 kN load cell. A displacement controlled tensile load was applied with a rate of 0.5 mm/min. To prevent slippage in the clamps, a 6 bar clamping pressure was applied and the end tab surfaces were roughened. In total, five straight and seven saw-tooth specimens were tested until catastrophic failure. Tests were accompanied by high speed camera (HSC) recordings in order to capture damage and modes of failure initiation and catastrophic breakage. A Photron SA-1 high-speed video camera equipped with a Nikon Micro-Nikkor 105 mm f2.8 type lens was used, where the field of interest was the specimen's edge in the tapered zone.

3. Results

3.1. Composite layup modelling

Fig. 4 shows a series of stacking sequences that was evaluated by simulation. For simplicity, only one half of the symmetric layup is illustrated. The locations of the predicted delamination failure initiation are indicated by the yellow circles. Note that only a delamination initiation failure at ± 45° ply drop is considered as valid failure mode. Hence, acceptable configurations are those with the yellow circle located at a green or blue shaded ply.

Sequence number 1 was adopted from Kawashita et al. [13] and served as the initial design in this study. This design exhibits a nearly symmetric thick and a symmetric thin section. Furthermore, four of the 8 ply drops have been realised by 0° plies. In order to avoid delamination initiation at a 0° ply and to obtain a delamination failure at a ± 45° ply drop, the more compliant ± 45° plies needed to be terminated closer to the thin section, which is the location of the first ply drop and delamination initiation. Therefore, various stacking sequences were developed (2 to 8) and their modelled failure behaviour and ultimate tensile strength analysed. The created layups were both symmetric in the half laminate at the thick and thin sections (as indicated by the S symbol in Fig. 4) and balanced in order to avoid membrane/bending and bending/twisting coupling.

The obtained results are further discussed in more detail with respect to the requirements on strength, failure mode and failure location in the following section.

3.2. Maximum load and failure

Fig. 5(a) shows the modelled tensile failure stresses of the stacking sequences introduced in Fig. 4. Due to the ply drops, interface ele-

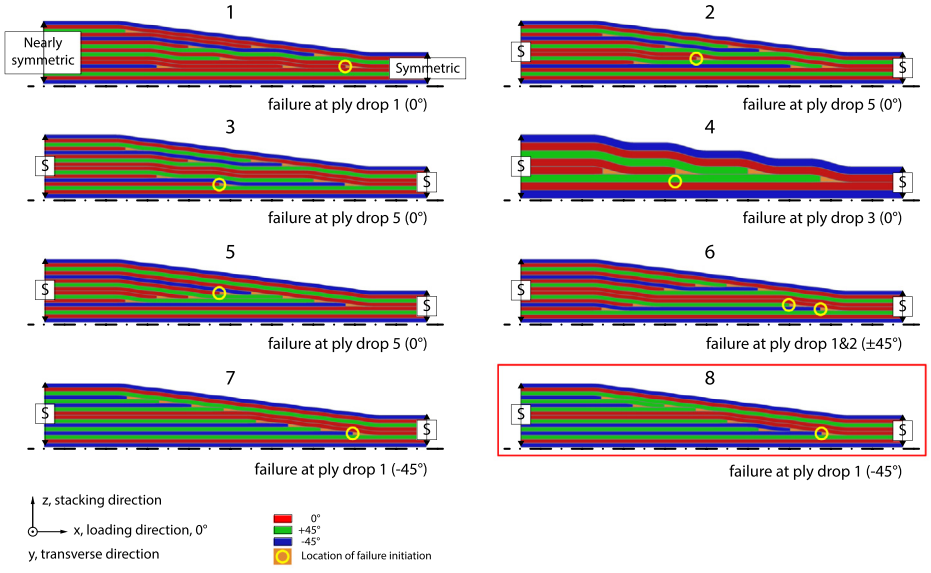

Fig. 4. Stacking sequences and ply drop designs, showing one half of the symmetric specimen. The 'S' symbol indicates the symmetry of the local layups in the thick and thin sections. The yellow circles indicate locations of predicted delamination initiation. Stacking sequence number 8 was selected for mechanical experiments. (For interpretation of the references to colour in this figure legend, the reader is referred to the web version of this article.)

ments in the critical zone of the taper, i.e. close to the thin section, experience locally high interlaminar stresses. Such high stresses trigger delamination failure at a relatively low global stress level, at which the fibres are still intact.

Stacking sequences number 1 to 3 exhibited high failure loads but the delamination failure was initiated at a 0° ply drop. The 0° ply drops cannot be created with the saw-tooth pattern and thus needed to be disregarded as a viable failure location for this study. The stacking sequence number 3 was found to be an exception. Indeed, initial softening occurs around the first 0° ply drop, i.e. ply drop 5. However, catastrophic failure seems to be happening afterwards at the ply drop 1, which is an off-axis ply drop. The proximity of both events was the reason why the failure of stacking sequence 3 was considered as 0° ply drop failure. The failure stress of stacking sequence number 4 was found to be lower due to the high thickness of the blocked plies that are dropped at the same location. This reduced the stress level at which delamination failure occurs [9,16,28].

Because of their high stiffness, dropped plies with an unidirectional fibre orientation are much more susceptible to delamination than off-axis plies [16,20]. During the design phase, dropped 0° plies were progressively moved towards the thick section of the taper to allow for the delamination failure at ± 45° angle-plies (see stacking sequences 5 and 6 in Fig. 4). Delamination occurred at the 5th and first ply drops in stacking sequences 5 and 6, respectively. Despite configuration

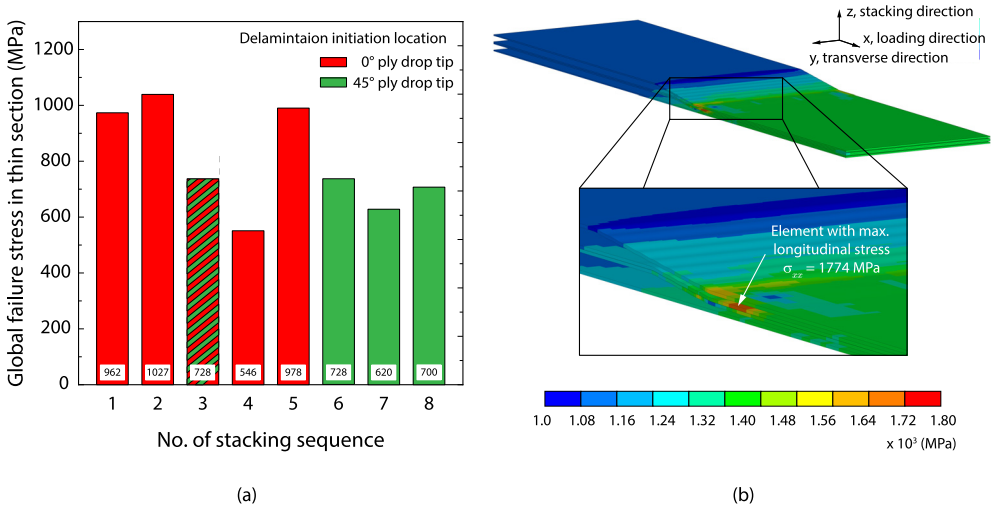

Fig. 5. (a) Modelled failure stresses of developed stacking sequences. Green columns indicate sequences in which delamination failure initiated at ± 45° ply. (b) Longitudinal fibre stress in stacking sequence number 8 at delamination initiation. (For interpretation of the references to colour in this figure legend, the reader is referred to the web version of this article.)

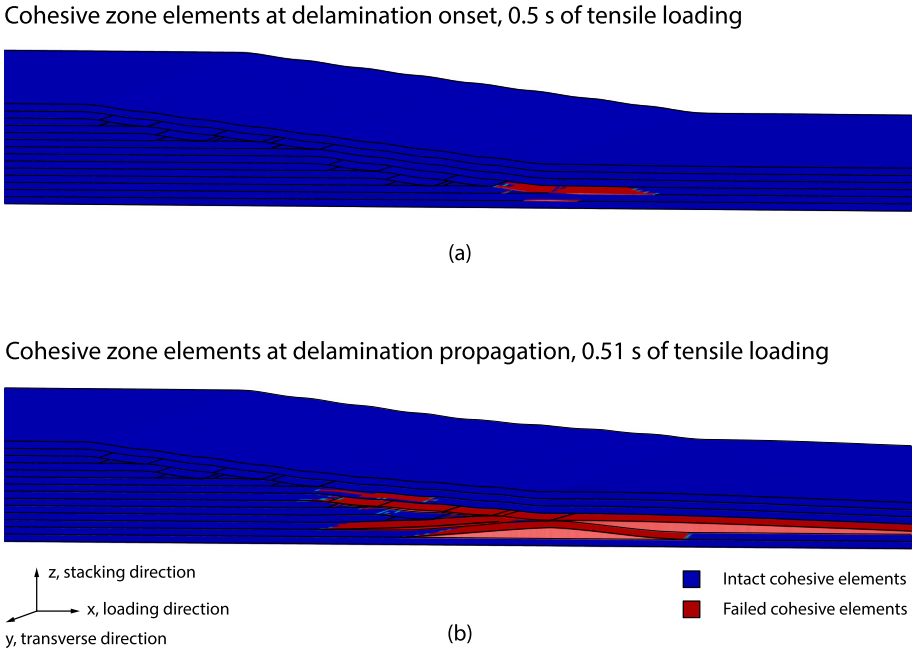

Fig. 6. Cohesive zone elements of stacking sequence number 8 at (a) onset of delamination at 0.5 s of tensile loading and (b) delamination propagation at 0.51 s.

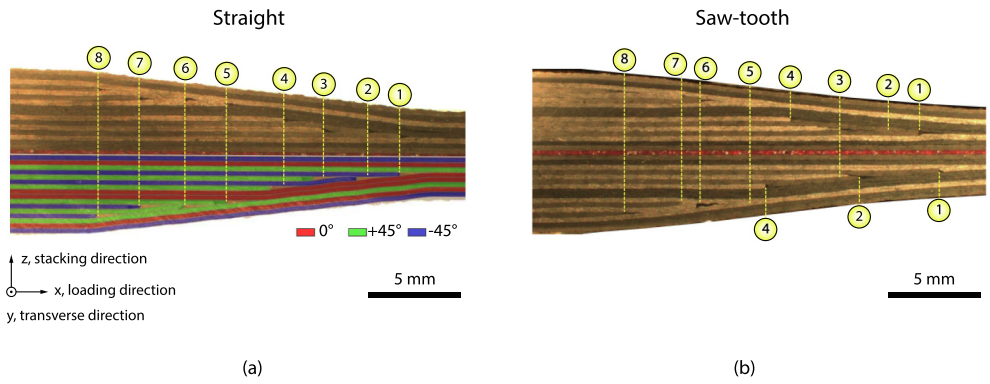

Fig. 7. Microscopy images of tapered zone of (a) straight and (b) saw-tooth specimens, with numbered ply drops starting from the thin end.

number 6 exhibited the desired failure behaviour, the close proximity to failure that also initiated at the first 0° ply drop led to the creation of stacking sequences 7 and 8. In these two configurations, 0° ply drops were avoided and the thickness change was only realised with ± 45° ply drops.

Fig. 5(b) shows the fibre direction stress, σ_{11}, at delamination failure for stacking sequence 8. The fibre direction stress magnitude at which the delamination was initiated is below the manufacturer's data sheet strength of 2724 MPa [26], indicating that failure would occur first by delamination in physical tests.

To assess the delamination behaviour, the responses of the cohesive elements were closely monitored. The cohesive element failure flag (FF) is a parameter that indicates the state of the cohesive elements. Per definition, the FF is zero when the stresses are below the mixed-mode initiation criterion (Eq. (1)). The FF takes the values between 0 and 1 for damage evolution, and finally the value 1 for element failure.

Fig. 6 shows the progressive failure of the cohesive zone elements at (a) onset of delamination at 0.5 s of tensile loading and (b) delamination propagation at 0.51 s. Only the interfacial layers modelled with cohesive zone elements are shown, with the plies, modelled as solid elements, blanked.

After studying the results of the FE analyses of the different possibilities, there was little to choose between stacking sequence 7 and 8. Stacking sequence 8 was selected for manufacture of specimens for the experimental study due to adjacent plies not being dropped consecutively along the length of the specimen (as is the case in 7), which is closer to industrial practice.

3.3. Composite morphology

Fig. 7 shows micrographs of cut sections in the length direction of the two manufactured composite configurations using the ply drop distribution of stacking sequence number 8. Fig. 7(a) illustrates the configuration with straight ply drops including a direct comparison with the idealised design and Fig. 7(b) shows the same configuration with saw-tooth ply drop tips. The very good agreement of ply drop positions between the specimen and the model indicates that the manual layup can be done accurately. In addition, the two halves could be positioned precisely, leading to a very good alignment of the ply drops. Because of the higher complexity, an equally good alignment of the ply drops in the saw-tooth configuration was harder to obtain. In Fig. 7(b), the same ply drop on each side of the bonded halves do not precisely align, but this may be a function of exactly where the section cut is taken across the saw-tooth profile of the different plies. The offsets were still found to be comparatively small with a maximum value of 1.3 mm of ply drop number 2.

3.4. Effect of ply drops on tensile properties

Fig. 8 shows the applied thin section tensile stress-displacement curves of the ply drop samples with straight (blue curves) and saw-tooth ply drop tips (red curves). The numerically modelled stress at delamination initiation, determined by the nominal ply drop distribution of stacking sequence number 8 (see Figs. 4 and 7(a)) and the cohesive element strength pair of [90 MPa, 110 MPa], is illustrated as a horizontal dashed line for comparison. It should be noted that the 'strength pair' notation refers to mode I and mode II initiation stress S_I and S_{II}, respectively, as defined in Eq. (1) (see Section 2.2). The experimental curves reveal that both the tensile stiffness, E_t, and the ultimate tensile failure stress, σ_{tmax}, between the straight and the saw-tooth specimens are very similar (see values in Table 3). The slope of the linear part of the stress-displacement curves was used to represent the initial stiffness, E_t.

The average initial stiffness of the straight ply drop specimens was measured to be 63 GPa. In contrast, the stiffness of the saw-tooth ply

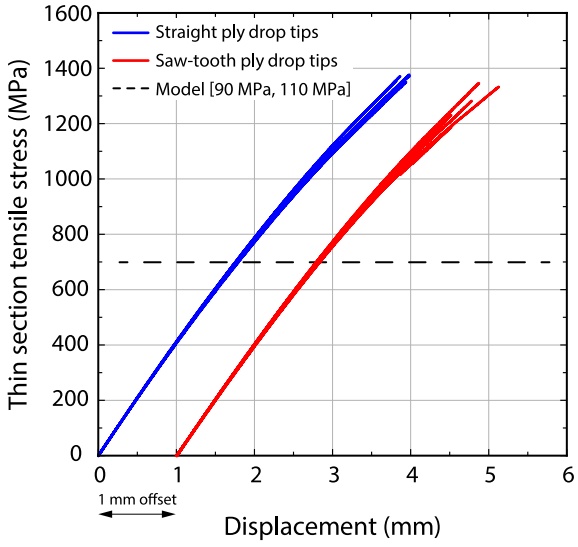

Fig. 8. Tensile applied thin section stress-displacement curves of tapered specimens with straight (blue), saw-tooth (red) ply drop tips. Nominal modelled delamination initiation stress (cohesive strength pair of [90 MPa, 110 MPa]) is shown with the dashed horizontal line. Offset of 1 mm was use for easier comparison of the two sets of curves. (For interpretation of the references to colour in this figure legend, the reader is referred to the web version of this article.)

drop samples was found to be 61 GPa, representing a reduction of less than 1%. Although, the calculation of the stiffness using the cross-head displacement is less accurate, the values are viable for a comparison since specimen slippage was not observed and the testing machine compliance remained constant.

The ultimate tensile stresses were measured to be 1355 and 1229 MPa for the straight and the saw-tooth ply drop specimens, respectively. By considering the standard deviations of both measurements, no significant difference was found between the two types of specimens. The differences in strength is higher than in modulus, whereby the saw-tooth average strength is about 10% lower than the strength of the straight specimens. In addition, a higher standard deviation was calculated for the strength of the saw-tooth samples, most likely due to geometrical differences amongst the specimens. The test coupons were extracted from a broad plate and it is possible that the distribution of the saw-tooth shape of the ply drops was not consistent amongst the specimens.

The loading response of both types of specimens was initially nearly linear-elastic (Fig. 8). Upon further loading, a slight non-linearity within the load–displacement curve was recorded. The non-linear behaviour can be attributed to the presence of angle-plies, which are susceptible to matrix cracking and non-linearity at a comparatively early stage in the mechanical test. Slippage of the sample, which could also be a potential source for deviations from a linear-elastic stress response, was not found. Matrix cracking failure of the 45° off-axis plies, in particular those located at the specimen's surface, clearly preceded the final failure. These premature damage events were noticed by audible sounds and surface ply peel-off effects.

3.5. Effect of ply drops on failure behaviour

The predicted failure mode of stacking sequence number 8 was a delamination failure with damage initiation at ply drop 1, which is a −45° ply (see Fig. 7). To validate the modelling results and to study differences between the composite configurations, the mechanical tests were accompanied with high speed camera (HSC) recordings at a frame rate of 285,000 frames per second. Fig. 9 shows a series of frames recorded prior (frames (a) and (b)) and during the failure event of a specimen with straight ply drop tips. Fig. 9 (c) represents the onset of failure and illustrates the location of damage, indicated by the blue circle. Interestingly, the predicted failure mode, i.e. delamination, could not be observed on the specimens with straight ply drops. For the case of the shown series of HSC frames, the final failure was initiated through fibre failure in the blocked 0° plies on the left side of the sample, which appear as brighter layers. The progression of failure as shown in Fig. 9(d)–(g) is characterised by fibre failure on the left side of the specimen and delamination as a result of the stress concentrations created by the preceding fibre damage. Hence it can be stated that delaminations occurred after the fibre failure.

Fig. 10 shows an HSC image series of a specimen with saw-tooth ply drop tips. The type of failure mode and the location of failure initiation is illustrated in Fig. 10(c) by a red circle. In this case, and different to the straight ply drop sample shown in Fig. 9, a delamination failure type occurred between the blocked 0° plies and −45° ply drop 1, which is the ply dropped closest to the thin section of the taper. This behaviour was observed for all specimens with the saw-tooth ply drop pattern. Delamination developed at ply drop tip 1 and rapidly propa-

Table 3
Measured tensile properties of tapered specimens with straight and saw-tooth ply drop tips. E_t represents the stiffness, σ_{tmax} the strength and the CV of σ_{tmax} the coefficient of variation of the measured strength.

Configuration	Number of tests	E_t(GPa)	σ_{tmax}(MPa)	CV of σ_{tmax} (%)
Straight	5	63 ± 0.4	1355 ± 19	2.4
Saw-tooth	7	61 ± 0.6	1229 ± 98	8.0

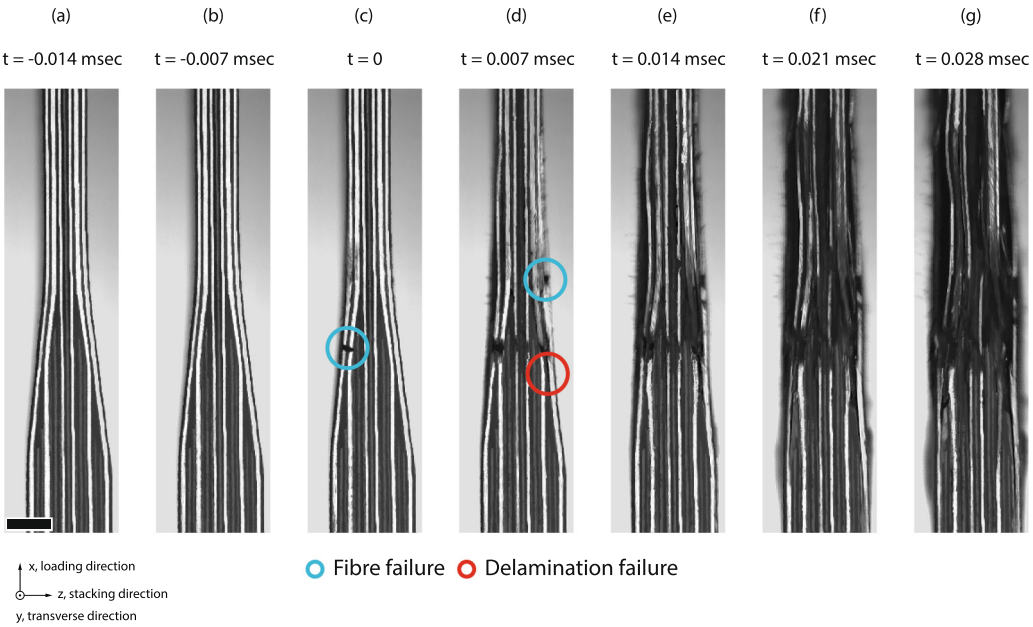

Fig. 9. High speed camera frames: Failure events of a specimen with straight ply drop tips. The location of fibre failure initiation is indicated by the blue circle, whereas subsequent delaminations by the red circle. The scale bar in frame (a) represents 4 mm. (For interpretation of the references to colour in this figure legend, the reader is referred to the web version of this article.)

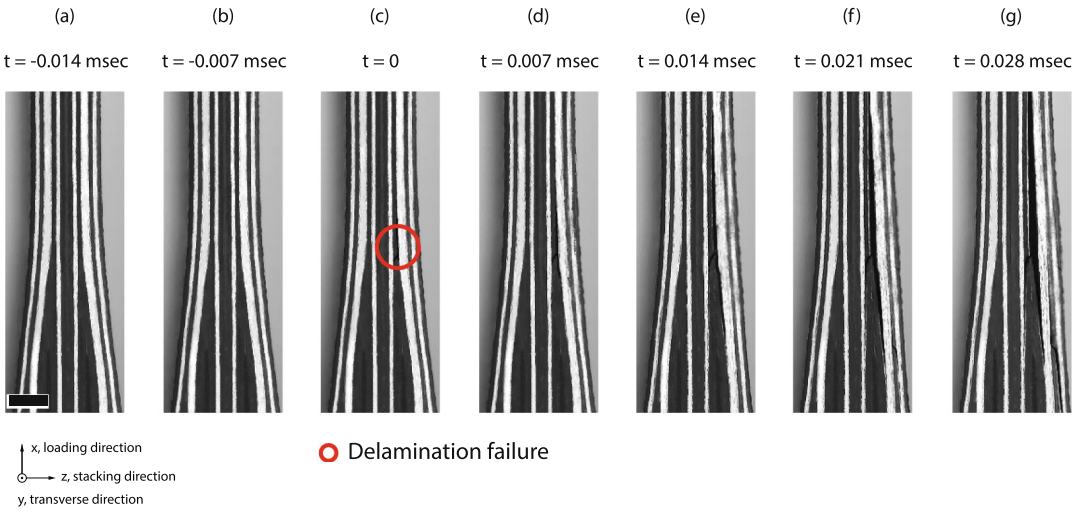

Fig. 10. High speed camera frames: Failure event of a specimen with saw-tooth ply drop tips. The location of delamination failure initiation is indicated by the red circle. The scale bar in frame (a) represents 2 mm. (For interpretation of the references to colour in this figure legend, the reader is referred to the web version of this article.)

gated along the interfaces between the continuous and discontinuous plies. After initiation, the delamination propagated along this 0°/45° interface in both directions as shown in Fig. 10(d)–(f) for a typical specimen. This failure mode is consistent with the model results.

4. Discussion

The model from Zhang et al. [15] was used to develop the tapered composite layups that were expected to fail by delamination, initiated at a ± 45° ply drop. Amongst the progressively developed layups (Fig. 4) stacking sequence number 8 showed the desired failure behaviour, which also indicated that delamination clearly precedes fibre failure. Local fibre direction stresses prior to the predicted failure were compared to the theoretical strength value. It was found that initial trial stacking sequence 1 did not meet the requirements. This model exhibited delamination failure at a 0° ply drop. In order to achieve delamination initiation at a ± 45° ply drop, the layup was modified according to design guidelines found in the literature [7,16]. Firstly, the order of dropped plies was changed so that the stiff 0° plies with a greater susceptibility to delamination were dropped before the more compliant ± 45° off-axis plies (see stacking sequences 2 to 6). Subsequently, the UD plies that carry the majority of the load were completely neglected as dropped plies. In the absence of ply drops with 0° fibre orientation, the requirements on the failure mode and location could be met with stacking sequences 7 and 8. The delamination initiation criterion (Eq. (1)) was satisfied at the location of ply drop tip 1 and the local stresses were found to be below the material's strength. The stacking sequence number 8 was then chosen for the manufacture of the straight and the saw-tooth test specimens.

The tensile tests revealed that the difference in stiffness between the two composite configurations is negligible (see Fig. 8 and Table 3). The nominal layup is identical and it seems that in the low strain region there is no effect of the saw-tooth ply drop pattern on the stress–strain response. In addition, the effective far-field laminate stiffness falls between the equivalent laminate moduli for the thin and the thick section using classical laminate plate theory. The thin and thick sections of stacking sequence 8 have a theoretical stiffness of 91 GPa and 55 GPa, respectively. The measured stiffness of 63 GPa relates to a specimen considering half the amount of dropped plies.

The tensile strength was found to be more affected by the ply drop topology than the stiffness. Average values of 1355 MPa and 1229 MPa were measured for the samples with the straight and saw-tooth ply drops, respectively (Fig. 8). This corresponds to a knockdown factor of about 10%. Larger resin rich zones were created because of the saw-tooth formation. This may have led to a locally lower fibre volume fraction and to higher susceptibility to prematurely develop cracks. Furthermore, the saw-tooth pattern causes waviness of the plies above and below the terminated ply, not only in the longitudinal direction but also in the width direction (see Fig. 2(b)). These could be reasons for the reduction in strength. The increase in standard deviation in strength can most probably be attributed to differences in the saw-tooth formation between specimens, due to difficulties to align the ply drop tips accurately (Fig. 7). The measured average tensile strength was found to be 94% higher for the straight and 76% higher for the saw-tooth configurations compared to the strength predicted by the initial numerical model (see Fig. 8).

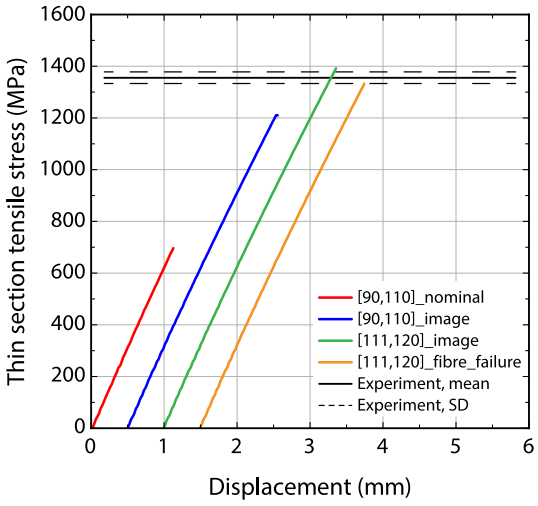

Fig. 11. Modelled stress-displacement curves of tapered specimens with various mode I and mode II cohesive element strength pairs. The values in the square brackets indicate the mode I and mode II strength in MPa. The black horizontal line represents the measured strength. Offset of 0.5 mm was use for an easier comparison of the sets of curves.

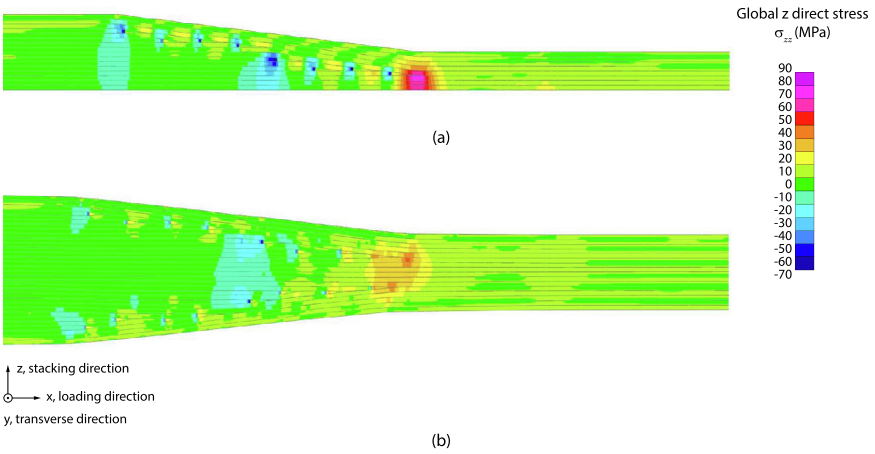

Fig. 12. Through-thickness direct stress just before failure of the (a) original mesh model, (b) image-based mesh model, at the same load.

To better understand this discrepancy between test and models, the input parameters of the cohesive elements in the models were varied, since there is some debate in the literature about the best values to use. In particular, the mode I and mode II strength pairs of the cohesive elements were varied. Simulations of the increased strength pairs, i.e. [90 MPa, 110 MPa], [100 MPa, 120 MPa] and [111 MPa, 120 MPa] were analysed. In addition, for these analyses, the finite element mesh was created directly from the ply paths on a specimen scanned cross-section edge, to accurately model the ply drop locations in a full model, without assumed perfect symmetry, as was done in references [13,15]. This is referred to as the 'image-based' mesh hereafter. This was not possible during the specimen design phase, before physical specimens were available. The fibre direction stress in the zero plies was reviewed as before. Fig. 11 depicts the obtained stress-displacement curves for the previous prediction with nominal ply drop positions and the new image-based mesh predictions, with various strength pairs. One can see that the delamination strength of the model with the initially used strength pair of [90 MPa, 110 MPa] has increased significantly in the image-based model. All other parameters have remained the same, indicating that minor geometric effects can be very significant. A smoother profile of the plies in the real specimens, i.e. less fibre waviness than in Fig. 4, can explain the difference in delamination strength.

The difference in delamination strength is especially noticeable in terms of the through-thickness stress concentration at the transition from the taper to the thin section. Fig. 12 shows ply local material through-thickness stress just before failure in the original model (Fig. 12(a)), compared to the new image-based model (Fig. 12(b)) at the same load. The through-thickness stress at this location, which contributes to the failure of the cohesive interface elements (Eq. (1)) is almost double in the original model, compared to the image-based mesh, which failed at a much higher load. Also, the angle of taper is slightly less steep in the image-based mesh, which is known to affect the strength [15]. The loss of precise symmetry as a result of layup inaccuracies in the real specimens is also captured in the image-based model, where no symmetry plane was used. This also contributed to the observed differences between the models.

Enhancing the strength pairs further increases the predicted strength, eventually exceeding the straight ply drop tip experimental result for the highest cohesive strength input. In this last case, it was notable that the modelled stress in the load bearing zero direction plies exceeded the manufacturer's data sheet value for fibre strength of 2724 MPa [26]. If the load–displacement curve is truncated at the point at which this strength value is exceeded (curve labelled "[111,120]_fibre_failure" in Fig. 11), then the numerically predicted result can be seen to be very accurate.

It is worth noting that for the [111 MPa, 120 MPa] strength pair case, the fibre failure and delamination predictions are close to each other, both almost within the experimental scatter. The experimental results of the straight ply drop drops follow the fibre failure prediction (see Fig. 9). On the contrary, for the saw-tooth ply terminations, it would appear that the perturbation of the ply termination geometry is sufficient to cause enough of a defect to bring the delamination failure load below that of fibre failure and change the failure mode (Fig. 10).

Previous tapered laminate model results have reported a relatively small sensitivity to the chosen cohesive strength pair data for similar geometries [15]. The change in behaviour observed here is attributed to the stiffness of the ply being terminated. In [15], failure always initiated at a 0° ply termination, where there was a high stress concentration and thus a fracture energy dominated behaviour. Hence, the failure is less sensitive to initiation stress. In the case of the more compliant 45° termination, as studied in this paper, the stress concentration will be less severe and so the failure will be more strongly affected by the ambient stress condition surrounding the ply termination.

5. Conclusions

Tapered composites with internally dropped plies designed to mimic realistic off-axis ply formations, as would occur in Automated Fibre Placement produced composites, were tested and compared to idealised ply drops. Specimens with saw-tooth ± 45° tips showed a change in the failure mode. The final failure of these specimens was initiated by delamination, whereas fibre failure was recorded for the straight ply drop tips. No significant change was found for the stiffness, whereas the average ultimate tensile strength was reduced by ~ 10% for the saw-tooth specimens. This confirms the initial assumption that the ply termination geometry will influence the local stress state, making the critical region of the taper more susceptible to delamination failure, although the measured effects were ultimately quite small. This result is significant for tapered laminated manufactures by AFP for structural applications.

Finite element models using only straight ply drop tip geometry and cohesive interface elements were used to determine the initial layup used in the tests, designed to fail by delamination from a 45° ply drop. Although the initial model predicted very conservative

strength values compared to the subsequent test results, it was still useful for specimen design and comparative analysis between candidate layups. The failure mode of the saw-tooth ply drop specimen experiments followed the predicted delamination failure mode and location, as shown by the series of high-speed camera images. The straight ply drop tip experiments however did not follow the predicted delamination failure mode and instead failed by fibre failure. A more precise finite element analysis of the layup used in the experiments was then able to explain this switch in failure mode. In the case of 45° ply drops, the model results are more sensitive to the cohesive element initiation strength values than in previous work. Modelling of the realistic geometry in tapered composites is important for an accurate predictive result, which can guide manufactures to adjust processes to obtain the best structural performance.

CRediT authorship contribution statement

Wilhelm Woigk: Methodology, Validation, Data curation, Writing - original draft, Writing - review & editing, Visualization. **Bing Zhang:** Methodology, Software, Validation, Writing - review & editing. **Mike I. Jones:** Methodology, Data curation. **Moritz Kuhtz:** Writing - original draft. **Andreas Hornig:** Writing - original draft. **Maik Gude:** Supervision. **Stephen R. Hallett:** Conceptualization, Software, Resources, Writing - original draft, Writing - review & editing, Supervision, Project administration, Funding acquisition.

Declaration of Competing Interest

The authors declare that they have no known competing financial interests or personal relationships that could have appeared to influence the work reported in this paper.

Acknowledgements

The authors would like to acknowledge Rolls-Royce plc for the support of this research through the Composites University Technology Centre (UTC) at the University of Bristol (UK) and the UTC for Lightweight Structures and Materials and Robust Design at the Technische Universität Dresden (Germany). We would also like to thank Dr Rafael Luterbacher Mus and Ms Alessia Kober for the great support and inspiring discussions.

References

[1] Lukaszewicz DHA, Ward C, Potter KD. The engineering aspects of automated prepreg layup : History, present and future. Compos Part B 2012;43:997–1009. https://doi.org/10.1016/j.compositesb.2011.12.003.
[2] Potter KD. Understanding the origins of defects and variability in composites manufacture. 17th Int Conf Compos Mater, 2009.
[3] Li X, Hallett SR, Wisnom MR. Modelling the effect of gaps and overlaps in automated fibre placement (AFP)-manufactured laminates. Sci Eng Compos Mater 2015;22:115–29. https://doi.org/10.1515/secm-2013-0322.
[4] Blom a. W, Lopes CS, Kromwijk PJ, Gurdal Z, Camanho pp. A Theoretical Model to Study the Influence of Tow-drop Areas on the Stiffness and Strength of Variable-stiffness Laminates J Compos Mater 43 2009 403 25 10.1177/0021998308097675
[5] O. Falcó J. Mayugo a., Lopes CS, Gascons N, Costa J. Variable-Stiffness Composite Panels: Defect tolerance under in-plane tensile loading Compos Part A Appl Sci Manuf 2014 10.1016/j.compositesa.2014.03.022
[6] Woigk W, Hallett SR, Jones MI, Kuhtz M, Hornig A, Gude M. Experimental investigation of the effect of defects in Automated Fibre Placement produced composite laminates. Compos Struct 2018;201:1004–17. https://doi.org/10.1016/j.compstruct.2018.06.078.
[7] Gan KW, Allegri G, Hallett SR. A simplified layered beam approach for predicting ply drop delamination in thick composite laminates. Mater Des 2016;108:570–80. https://doi.org/10.1016/j.matdes.2016.06.105.
[8] He K, Hoa S, Ganesan R. The study of tapered laminated composite structures: a review. Compos Sci Technol 2000;60:2643–57. https://doi.org/10.1016/S0266-3538(00)00138-X.
[9] Thomas DM, Webber JPH. A design study into the delamination behaviour of tapered composites. Compos Struct 1994;27:379–88. https://doi.org/10.1016/0263-8223(94)90264-X.
[10] Allegri G, Kawashita LF, Backhouse R, Wisnom MR, Hallett SR. On the optimization of tapered composite laminates in preliminary structural design. 17th Int Conf Compos Mater 2009.
[11] Vizzini AJ. Influence of realistic ply-drop geometries on interlaminar stresses in tapered laminates. ASTM Spec Tech Publ 1995:467–85.
[12] Wisnom MR, Gustafsson M. Delamination in tapered laminates under tension with ply drops skewed at an angle to the load. 17th Tech Conf Am Soc Compos 2002.
[13] Kawashita LF, Jones M, Giannis S, Hallett SR, Wisnom MR. High fidelity modelling of tapered laminates with internal ply terminations. 18th Int Conf Compos Mater 2011:1–6.
[14] Khan B. Suppression of delamination at ply drops in tapered composites by ply chamfering. J Compos Mater 2005;40:157–74. https://doi.org/10.1177/0021998305053459.
[15] Zhang B, Kawashita LF, Jones MI, Lander JK, Hallett SR. An experimental and numerical investigation into damage mechanisms in tapered laminates under tensile loading. Compos Part A Appl Sci Manuf 2020;133:. https://doi.org/10.1016/j.compositesa.2020.105862105862.
[16] Wisnom MR, Jones MI, Cui W. Failure of tapered composites under static and fatigue tension loading. AIAA J 1995;33:911–8. https://doi.org/10.2514/3.12510.
[17] B.R. Vidyashankar Krishna Murty a. V. Analysis of laminates with ply drops Compos Sci Technol 61 2001 749 58 10.1016/S0266-3538(01)00010-0
[18] Fish JC, Lee SW. Delamination of tapered composite structures. Eng Fract Mech 1989;34:43–54. https://doi.org/10.1016/0013-7944(89)90241-5.
[19] Botting AD, Vizzini AJ, Lee SW. Effect of ply-drop configuration on delamination strength of tapered composite structures. AIAA J 1996;34:1650–6. https://doi.org/10.2514/3.13285.
[20] Mukherjee a, Varughese B. Design guidelines for ply drop-off in laminated composite structures Compos Part B Eng 32 2001 153 64 10.1016/S1359-8368(00)00038-X
[21] Cairns D, Mandell J, Scott M, Maccagnano J. Design and manufacturing considerations for ply drops in composite structures. Compos Part B Eng 1999;30:523–34. https://doi.org/10.1016/S1359-8368(98)00043-2.
[22] Curry JM, Johnsont ER, Starnes JHJ. Effect of dropped plies on the strength of graphite-epoxy laminates. AIAA J 1992;30. https://doi.org/10.2514/3.10938.
[23] Jiang W, Hallett SR, Green BG, Wisnom MR. A concise interface constitutive law for analysis of delamination and splitting in composite materials and its application to scaled notched tensile specimens 2007:1982–95. https://doi.org/10.1002/nme.
[24] Li X, Hallett SR, Wisnom MR. Predicting the effect of through-thickness compressive stress on delamination using interface elements. Compos Part A Appl Sci Manuf 2008;39:218–30. https://doi.org/10.1016/j.compositesa.2007.11.005.
[25] Mukhopadhyay S, Jones MI, Hallett SR. Compressive failure of laminates containing an embedded wrinkle; Experimental and numerical study. Compos Part A Appl Sci Manuf 2015;73:132–42. https://doi.org/10.1016/j.compositesa.2015.03.012.
[26] Corporation H. HexPly 8552. Prod Data Sheet 2016:1–6.
[27] ASTM International. ASTM D3039/D3039M–14 - Standard Test Method for Tensile Properties of. Polymer Matrix Composite Materials. 2014.
[28] Wisnom M, Jones M, Cui W. Delamination in composites with terminating internal plies under tension fatigue loading. Compos Mater Fatigue Fract Fifth 2009:486–486–23.. https://doi.org/10.1520/stp14031s.